TECHNICAL REPORT

Overview of sample environments for research use at the PETRA III Swedish Materials Science beamline

Gabriel Spartacus[1], Peter Hedström[1], Denise McCluskey[1], Tao Zhou[1] and Fredrik Eriksson[2]

[1] KTH Royal Institute of Technology

[2] Linköping University

February 2023

A copy of this report is available on cexs.kth.se/

Center for X-rays in Swedish Materials Science
Technical Report Series
“Overview of sample environments for research use at the PETRA III Swedish Materials Science beamline”
Gabriel Spartacus, Peter Hedström, Denise McCluskey, Tao Zhou, and Fredrik Eriksson
TRITA-ITM-RP 2022:3
February 2023
ISBN 978-91-8040-448-8

Preface

The Swedish Materials Science beamline at the PETRA III synchrotron in Germany is a Swedish research infrastructure that became operational during 2019. This Swedish infrastructure is operated by Deutsches Elektronen-Synchrotron (DESY). Operational costs are funded by the Swedish Research Council. The Swedish Research Council also finances the Center for X-rays in Swedish Materials Science to act as the academic host of the PETRA III Swedish Materials Science beamline.

The PETRA III Swedish Materials Science beamline is a high-energy X-ray instrument for materials characterisation. So that the properties and behaviours of diverse materials can be studied under a wide range of conditions, researchers often use sample environments to conduct experiments when using the beamline. Information about the sample environments that are potentially available for experiments at the Swedish Materials Science beamline, as well as the experiments that each sample environment enables, is therefore important to researchers.

Different organisations can potentially provide a sample environment. It takes time to find information, time to judge whether a given sample environment is useful for a particular experiment - and time to assess whether the sample environment can be used at the Swedish Materials Science beamline. This document therefore aims to make this task more straightforward.

This report catalogues eleven sample environments that have proven to be useable, or are judged to potentially be useable with modifications, at the PETRA III Swedish Materials Science beamline according to research application areas. The application areas are Thermal treatments, Electrochemistry, Catalysis, Thin films, Mechanical response of materials and Levitation. Such cataloguing means that researchers can now start their search for relevant sample environments by looking up a relevant research application area.

This report goes on to provide examples of experiments and results that were obtained using each of the catalogued sample environments in order to illustrate the type of research that can be undertaken at the PETRA III Swedish Materials Science beamline.

Citations and links to specifications, published research cases and the organisation that is responsible for a given sample environment, are also provided as a basis for researchers to proceed with their research planning.

Contents

1. Introduction

This technical report presents an overview of sample environments which are usable at the PETRA III Swedish Materials Science beamline (potentially requiring arrangement or development of the beamline layout). Alongside the description of each sample environment, illustrative materials science studies are presented that exemplify the use of these sample environments for *in situ* and/or *in operando* measurements.

The sample environments referenced in this report are available either:

- Directly at the Swedish Materials Science beamline at PETRA III.
- As pool equipment of PETRA III (shared between beamlines, and thus requiring prior booking). This pool of sample environments is managed by the Sample Environment and Extreme Conditions Science Infrastructure (labeled as "ECSI" in this document).
- Through collaboration with DESY Nanolab located at DESY, who require prior contact well in advance of the planned experiments (see Section 4). DESY Nanolab may also be able to prepare samples for use in the sample environments.
- Through collaboration with research groups in Sweden or abroad who may be willing to support wider use of the sample environment that their group has developed. In such cases, the sample environment listing includes the contact persons associated with the relevant Swedish research groups at https://www.cexs.kth.se.

Some key information about the equipment presented is also included, such as links to reference material where detailed specifications about the device is available. Examples of such references are the manufacturer's documentation, patents or scientific publications. For each of the sample environments, a summary of experimental parameters and research results is also presented, along a references to published articles.

The final sections of this report provide references to the relevant unit with DESY, or in cases where the sample environment has been developed by a research group, a link to the contact details of the research group's principle investigator.

It may be useful to know that in some cases it may also be possible to request sample preparation services e.g. from DESY Nanolab.

It should be noted that the availability and characteristics of the sample environments may evolve over time. Sample environments may be upgraded and new sample environments may become available. The information in this report is therefore valid as of January 2023. For updated listings of sample environments that are available from the Swedish Materials Science beamline, ECSI (PETRA III pool equipment) and DESY Nanolab, see the webpage links in Section 4 and contact information in Section 5.

2. Sources and methods

The content of this report was developed using the following sources and method.

Stage 1. Identification of Sample Environments

1. The publications listed on DESY's P21.1 and P21.2 webpages were reviewed to identify the sample environments that had already been successfully used at the Swedish Materials Science beamline.
2. Presentations made at the User Meetings of the PETRA III Swedish Material Science beamline were reviewed to identify additional sample environments e.g. sample environments that research groups had developed themselves.
3. If sample environments were developed by research groups, these groups were contacted to collect information about the sample environment. In some cases, this resulted in the recommendation to cite particular references.
4. The particular organisation that is responsible for each sample environment was contacted and the link to that sample environment's specifications was identified.

This resulted in the identification of 11 sample environments that have proven to be used at the PETRA III Swedish Materials Science beamline, or can potentially be used perhaps requiring arrangement or development of the beamline layout. The latter sample environments have been used at other beamlines at PETRA III as well as other large scale infrastructures such as ESRF.

The research possibilities enabled by using these 11 sample environments are documented by summarising information from 33 published articles in peer-reviewed scientific journals, patents and technical reports.

Stage 2. Categorisation of Sample Environments

The identified sample environments were then classified according to their experimental research area, with the following research categories being identified:

- Thermal treatments
- Electrochemistry
- Catalysis
- Thin films
- Mechanical response of materials
- Levitation
- Others

These categories, together with the number of sample environments identified for each category, are illustrated in Figure 1.

Stage 3. Report writing

Within these research categories, this report lists and describes sample environments. For each sample environment entry, there is a description of the type of research that was possible using that sample environment as well as technical details of the sample environment itself. These descriptions include references.

The information reported here focuses on the synchrotron based x-ray experiments. Nonetheless, the research presented in most of the papers also relies on laboratory research and perhaps the use of other large scale facilities. To focus on the research possibilities of the PETRA III Swedish Materials Science beamline, such other characterisation techniques and equipment are not presented here. Nonetheless, it is important to note that experimental results from those additional techniques are generally also critical to the research performed. The reader is therefore advised to consult the cited scientific articles.

For completeness, this report also complies the full citations of articles, patents and other relevant sources of information in Sections 4-6.

Delimitation

This report only presents sample environments that have already been used, or can be used with some modifications, at the PETRA III Swedish Materials Science beamline.

Several other sample environments are available and interested reader see information about these sample environments through the links available in Section 4. However, these have not yet led to published articles and so are omitted from this report. 4.

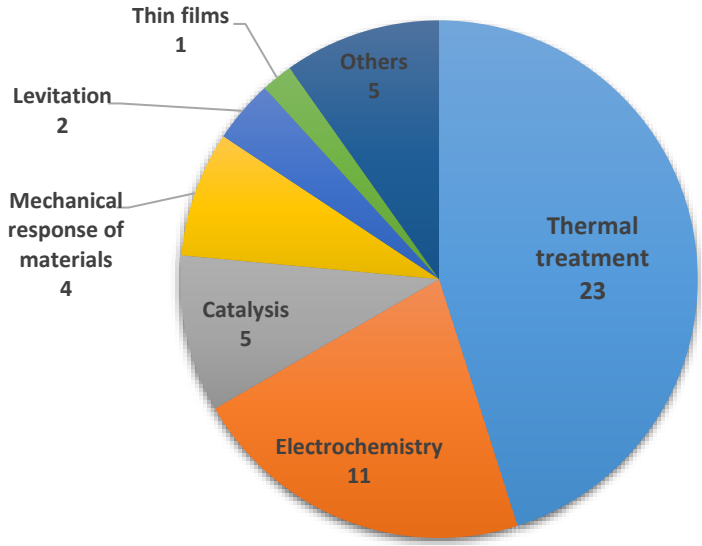

Pie chart classification of all the identified sample environments according to research application area, irrespective of whether they have a publish article arising from use of the PETRA III Swedish Materials Science beamline. Some sample environments may be used for in several categories of research areas.

3. Sample environments illustrated by research examples

Sample environments, and illustrative research use of each sample environment, are presented below according to the classified field of research.

3.1. Thermal treatments

Linkam furnaces (TS1500 @ P21.2 and THM600 @ECSI) | P21.2 & ECSI PETRA III Pool equipment

Jiang *et al.* used the THMS600 furnace in order to heat Cu-Zr-Al **metallic glasses** with various sulfur compositions (from 0 to 3 at.%), ramping up the heat in 0.333 K/s steps from room temperature up to ~ 800 K **[1]**. During the thermal treatment, X-Ray Diffraction (XRD) data was acquired *in-situ*. In this experiment, the temperature where the amorphous Cu-Zr-Al glass started to transform into $Cu_{10}Zr_7$ and FCC-τ_3 crystalline phases was probed with a time resolution of 5 s (corresponding to a temperature resolution of 1.665 K). These experiments enabled the identification of the rapid change in the primary crystalline phase that form depending on the sulfur content, which shift from a majority of Cu-Zr-Al eutectic phases to the fcc-τ_3 phase after addition of 0.75 at.% sulfur.

Using an **Fe-Cr system** with 30, 50 and 70 at.% of ferromagnetic Fe, Weissitsch *et al.* performed heat ramping at 10 K/min followed by an isothermal holding at 520 °C for 1 h and subsequent fast cooling during ***in-situ* XRD** **[2]**. The authors observed the grain size evolution and linked it to magnetic properties of the alloy. The experiments also allowed to show that no significant Fe-Cr demixing was present in the alloy after 1 h annealing at 500 °C (from the absence of broadening of the Fe-BCC peak and microscopy observations).

Wurster *et al.* investigated the magnetic properties of **nanocrystalline Cu-Co and Cu-Fe** by thermal treatment **[3]**. They performed ***in-situ* thermal treatment** and measured the microstructural changes (secondary phases, phase demixing, thermal dilatation…) by **XRD** during isothermal holding at different temperatures around 500 °C.

Experiments by the above authors were all performed at the Swedish Materials Science beamline, **P21.2** branch**.**

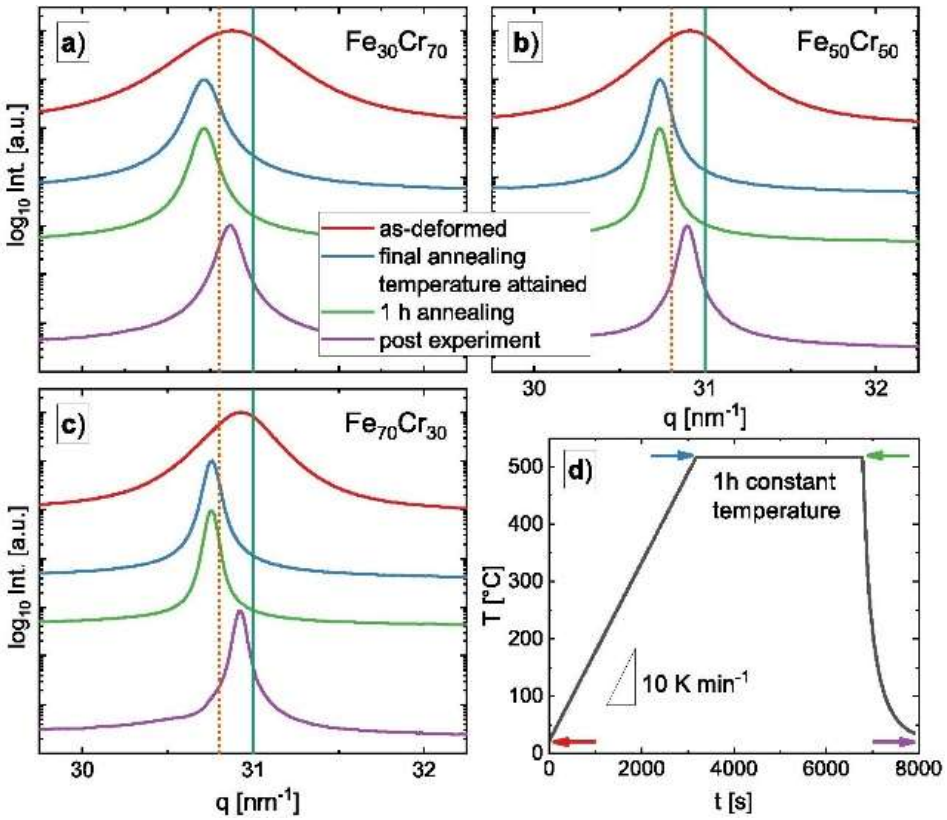

XRD patterns of $Fe_{30}Cr_{70}$ and $Fe_{50}Cr_{50}$ alloys displaying the peak shift and peak broadening evolution with temperature, from Weissitsch et al. 2021 [2], CC BY (Open access article).

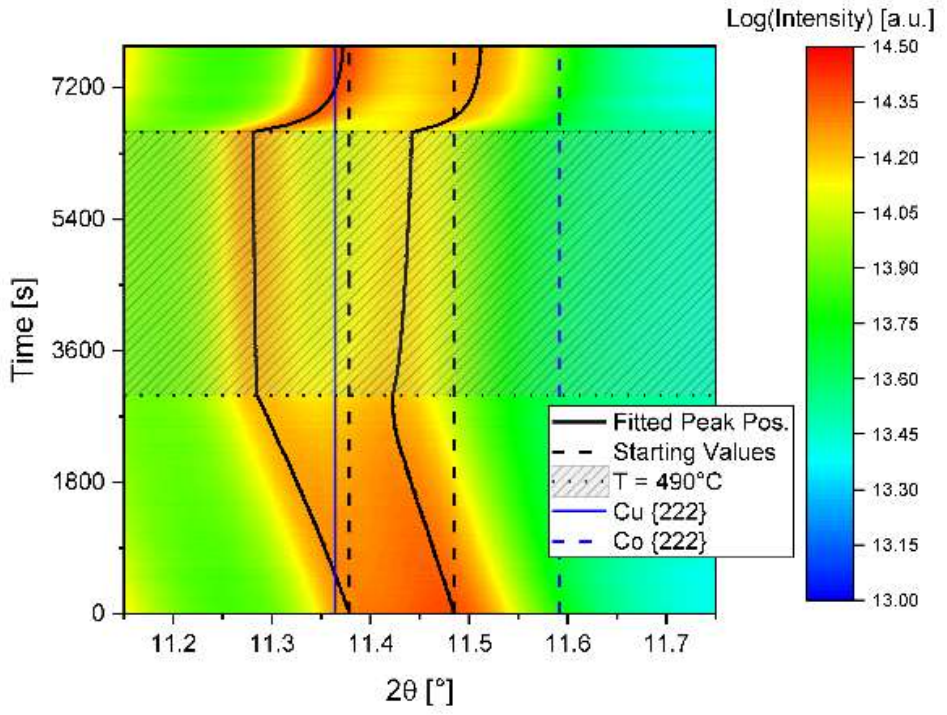

Evolution of the XRD patterns (at high angle only) of $Cu_{55}Co_{45}$ upon annealing up to 490 °C, from Wurster et al. 2020 [3] , CC BY (Open access article).

Further information about the sample environments

TS1500V manufacturer website: https://www.linkam.co.uk/ts-series-brochure-3

THMS600 manufacturer website: https://www.linkam.co.uk/thms600

Linkam TS1500V

Linkam THMS600

Courtesy of Linkam Scientific Instruments Ltd.

Solvothermal capillary reactor | P21.1

Broge *et al.* studied **High Entropy Alloys** (**HEA**), in **nanoparticle** form, for catalytic reactions **[4]**. The **scattering** of different HEA nanocatalysts under different temperature conditions were measured, where the temperature was increased stepwise up to 450 °C. Evolution of crystalline phases was analyzed in terms of unit cell and average crystallite size (extracted from peak broadening). **Pair Distribution Function** (**PDF**) of the dissolved precursors where acquired, which enabled characterisation of average atomic distances of the precursors molecules.

Experiments were performed at the Swedish Materials Science beamline, **P21.1** branch.

Further information on the sample environment:

P21.1 Sample environment webpage.

Description article: [5] J. Becker *et al.* (2010) J. Appl. Cryst., Vol.43, p.729–736. (https://doi.org/10.1107/S0021889810014688)

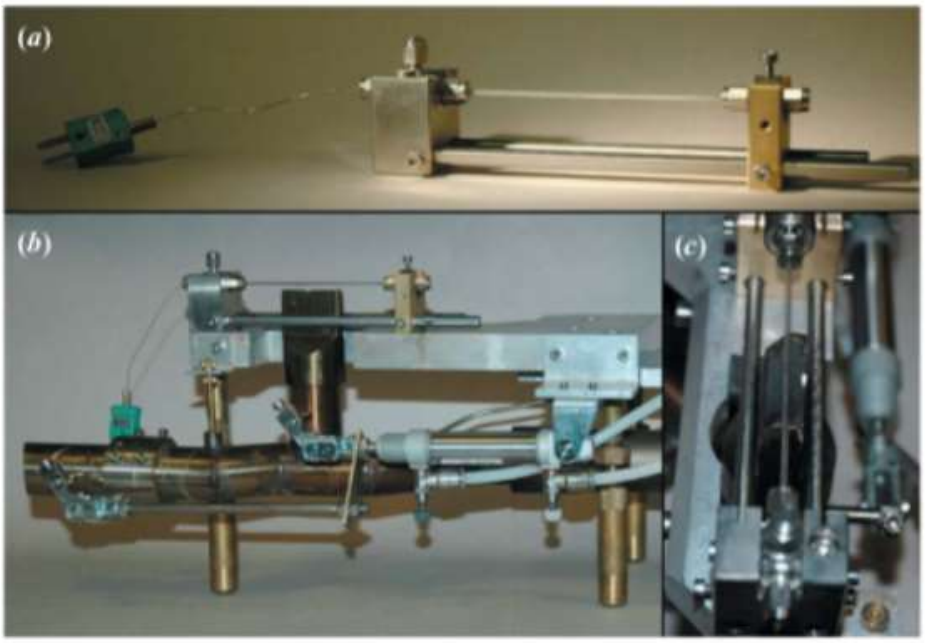

Picture of the sample environment, from Becker et al. 2010 [5], this figure is reproduced with permission of the International Union of Crystallography.

Rotating furnace | Lorraine University (France)

Benrabah *et al.* observed the difference in **ferrite phase fraction** in **steel,** where samples had a gradient in composition, during isothermal holds at different temperatures (between 700 °C and 800 °C) by ***in-situ*** **XRD**. This approach enabled the screening of phase transformation kinetics for a wide range of steel compositions within one ***in-situ*** **heat treatment** (high-throughput) experiment **[6, 7]**. The rotation capability of the furnace was especially interesting in order to average grains in diffracting condition and thus obtain clean powder pattern data.

Experiments were performed at the Swedish Materials Science beamline, **P21.2** branch**.**

Further information on the sample environment:

Patent: [8] B. Denand *et al.* (2021) https://hal.univ-lorraine.fr/hal-03451741.

Fast current induced heating devices for ribbon / bulk materials | IFW Dresden (Germany)

Orava *et al.* performed an ***in-situ*** **XRD study** of **Cu-Zr-Al metallic glasses** in order to map the **phase evolution with respect to temperature** [9]. **Ribbon samples** were used and followed a flash-annealing up to a **temperature of ~ 1200 K** where the **heating rate was ~1100 K/s**. The chamber was either under **vacuum** or flushed with **He** (allowing a faster cooling). Identification of the crystalline phases which form upon cooling was possible, including the dependence of cooling rate. This study also used an electromagnetic levitation device for *in-situ* XRD, described in ref. [10].

Experiments were performed at the Swedish Materials Science beamline, **P21.1** branch**.**

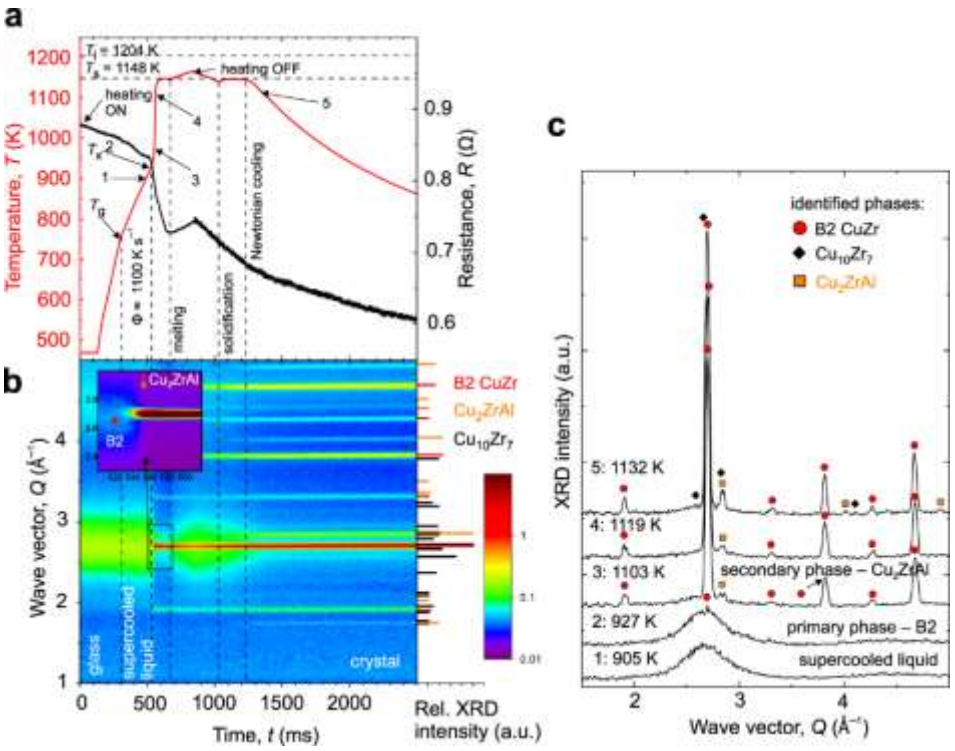

Diffraction pattern evolution showing the occurrence of crystalline phases during heating of the $Cu_{47.5}Zr_{47.5}Al_{5.0}$ metallic glass and subsequent cooling under vacuum, from Orava et al. 2021 [9] , CC BY (Open access article).

Further information on the sample environment:

Description article: [11] J. Orava *et al.* (2020) Rev. Sci. Instrum. Vol.91, No.073901 (https://doi.org/10.1063/5.0005732)

3.2. Electrochemistry

Electrochemical flow cell | DESY Nanolab

The Electrochemical flow cell available via DESY Nanolab has been used at both PETRA III and ESRF.

Zhang *et al.* studied the **anodization of aluminum alloys** (AA 6082 and AA 7075) **[12]**. Using this electrochemical cell, they performed *in-situ* **X-Ray Reflectivity** (**XRR**) during anodization at different applied potential (from open circuit potential to 3.7 V) to follow the evolution of the aluminum oxide film thickness over time. Qualitative trends of the roughness evolution within the aluminum oxide film thickness was also extracted. Experiments were performed at the **ID03 beamline** at **ESRF**.

Weber *et al.* studied the **anodic corrosion behavior** of a **single-crystalline film of IrO_2** supported by a slightly bulk-reduced TiO_2(110) single crystals by acidic water splitting **[13]**. They performed ***operando*** **XRR and Surface X-Ray Diffraction** (**SXRD**) during the corrosion reaction. The combination of these techniques allowed to follow the film stability, by following its thickness and structural evolution. Experiments were performed at the PETRA III Swedish Materials Science beamline, **P21.2** branch**.**

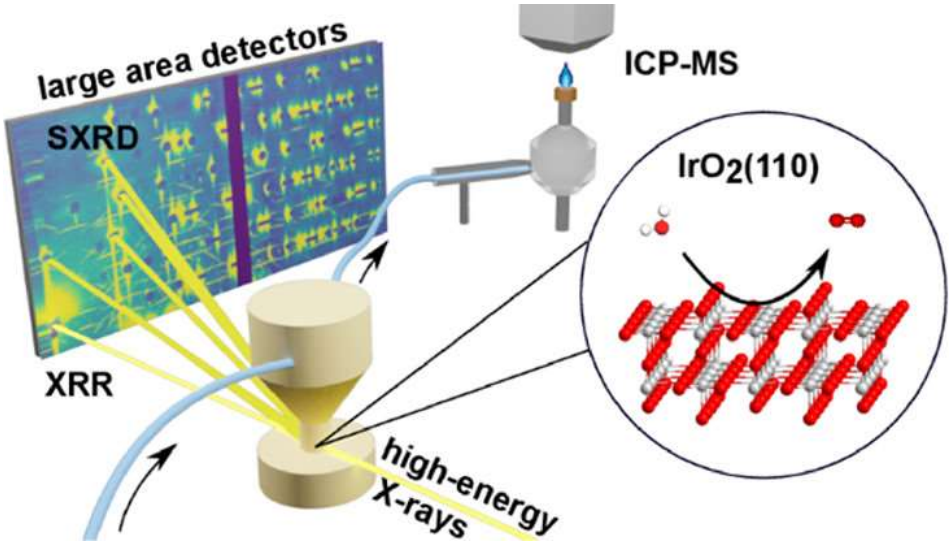

Experimental setup schematic, Reprinted with permission from T. Weber, V. Vonk, D. Escalera-López, G. Abbondanza, A. Larsson, V. Koller, M.J.S. Abb, Z. Hegedüs, T. Bäcker, U. Lienert, G.S. Harlow, A. Stierle, S. Cherevko, E. Lundgren, H. Over, ACS Catalysis 11 (2021) 12651–12660. Copyright 2021 American Chemical Society [13].

Further information about the sample environment:

Description article: [14] M. L. Foresti *et al.* (2006) *Electrochim. Acta*, Vol. 51, p.5532–5539. (https://doi.org/10.1016/j.electacta.2006.02.031)

Electrochemical cell with tensile load frame | KTH (Sweden)

This electrochemical cell within a tensile load frame was used by Örnek *et al.* to study the **lattice strain evolution** during electrochemical **hydrogen charging** and **mechanical loading** of a **duplex stainless steel** **[15,16]**. They performed ***in-situ*** **XRD** in order to follow the lattice strain in the austenite and ferrite phases. They also observed differences in the strain partitioning between the two phases.

Experiments were performed at the Swedish Materials Science beamline, **P21.2** branch**.**

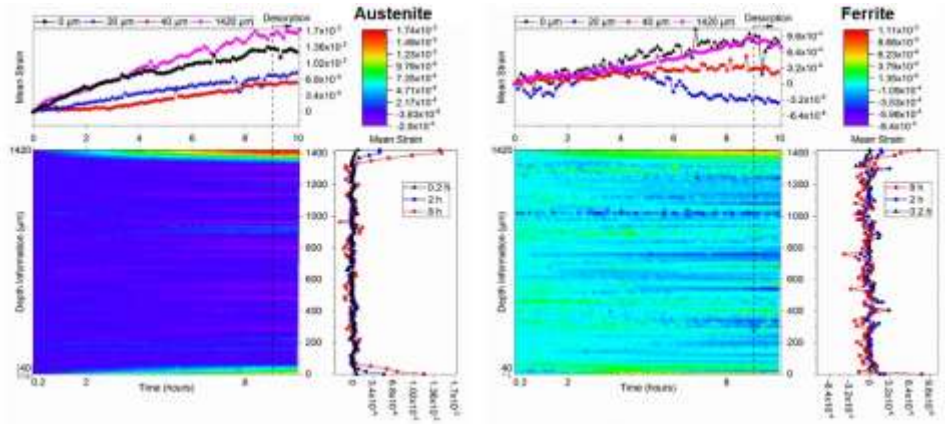

Time evolution of lattice strain in austenite (left) and ferrite (right) perpendicular to the loading axis. As time evolves so does also cathodic hydrogen charging and hydrogen desorption into the depth of the sample. The curves display the strain evolution at different depth and time, from [16] , CC BY (Open access article).

Further information about the sample environment:

Description article: [16] Örnek *et al.* (2020) *Corr. Science*, Vol. 175, p.108899. (https://doi.org/10.1016/j.corsci.2020.108899).

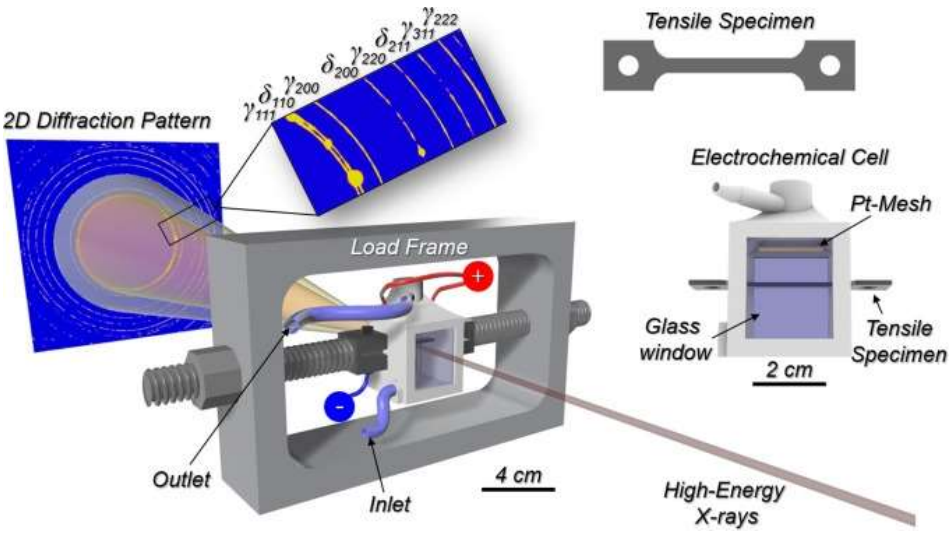

Schematic of the sample holder and experimental setup used, from Örnek et al. 2020 [16] , CC BY (Open access article).

Microscope with integrated LED light source | Lund University (Sweden)

This sample environment can be used together with a compatible electrochemical cell, or heating chamber. This optical microscope can perform 2D Surface Optical Reflectance (2D-SOR) observations, and is suitable for conducting **various surface characterisation** research studies such as thermal catalysis, electrocatalysis, and corrosion science. The wavelength of the light source depends on the chosen LED.

Linpé *et al.* performed 2D-SOR analysis on polycrystalline Al as well as on single crystals of Au (111) and Pt (100) **[17-19]**. Pfaff *et al.* studied the oxidation of CO on a **Pt (100) catalyst** and showed that the evolution of the reflectance of the Pt (100) catalyst can be correlated to the evolution of the oxide thickness and roughness. These results required simultaneous 2D-SOR and **SXRD *operando*** experimental measurements **[19]**. The Swedish Materials Science beamline, **P21.2** branch was used for several of these experiments**.**

A similar sample environment is also available at DESY Nanolab. DESY Nanolab, who require researchers to contact them well in advance of beam time proposals for feasibility check and experiment planning.

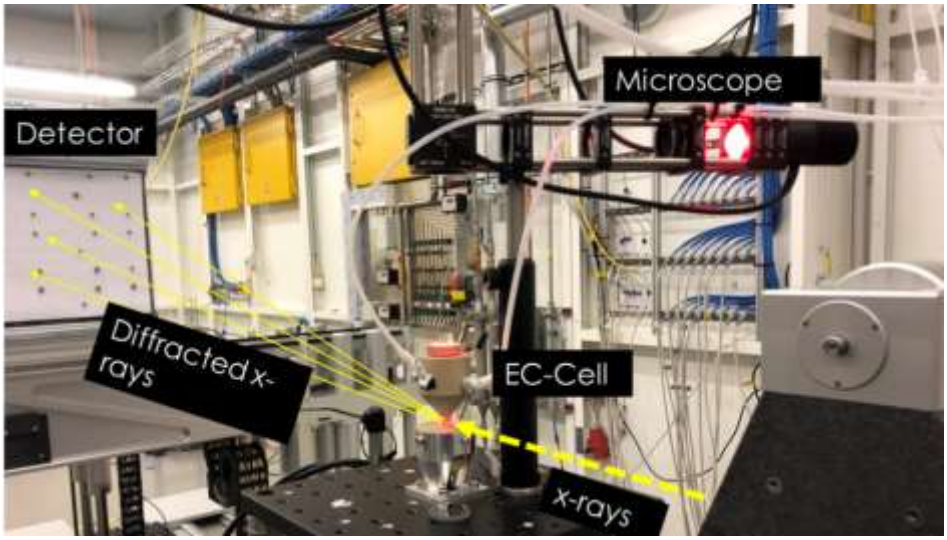

Photograph of experimental setup, curtesy of Dr. Gary Harlow, Lund University.

Further information about the sample environment:

Description article: [19] S. Pfaff *et al.* (2021*) ACS Appl. Mater. Interfaces* Vol.13, No.16, p.19530. (https://pubs.acs.org/doi/10.1021/acsami.1c04961)

Magnetic cryostat | P21.1

The magnetic cryostat available at the P21.1 beamline has been used by Galeski *et al.* for investigations of the **quantum Hall effect on $ZrTe_5$ semimetal**. Observations of **XRD** peaks of $ZrTe_5$ have been made with and without a **magnetic field up to 2 T**. These experiments demonstrated that the crystal structure did not display any changes in this range of magnetic field **[20]**. Experiments were performed at the Swedish Materials Science beamline, branch **P21.1.**

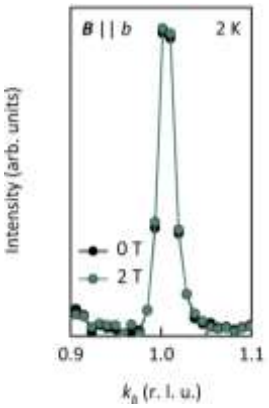

The (010) peak of $ZrTe_5$ observed by XRD, with and without 2 T magnetic field, displaying no structural changes, and no appearance of satellite peaks related to secondary phases, from Galeski et al. [20], CC BY (Open access article).

Further information about the sample environment:

Beamline website: P21.1 Sample environment webpage.

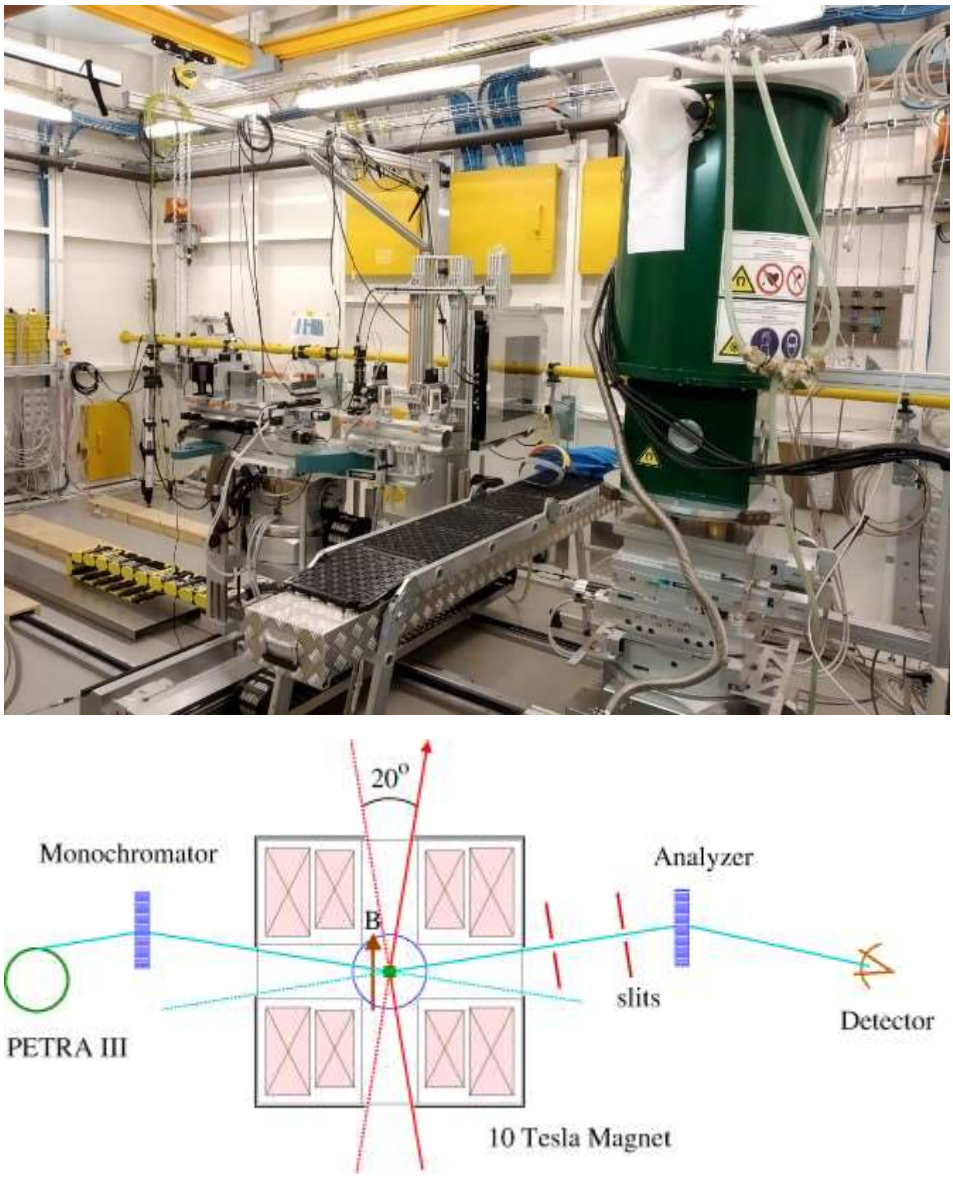

From the P21.1 sample environment webpage (January 2023).

Reactor cell | ETH (Switzerland)

This reactor cell can be used at several synchrotron and neutron facilities.

In their study, Staniuk *et al.* followed the complex mechanisms of **cobalt oxides** (**Co_3O_4** and **CoO**) as well as **Co nanoparticules** synthetization in an organic solvent. **XRD** and **X-Ray Absorption Spectroscopy** (**XAS**), performed ***in-situ* up to 180 °C** during the synthetization of Co oxide and Co nanopowders enabled the identification of the occurrence of four chemical reactions within the solvent, and the complex interdependence of these four chemical reactions was revealed **[21]**. Experiments were performed at the **Swiss-Norwegian Beamline** (**SNBL**) **BM01B** at **ESRF**.

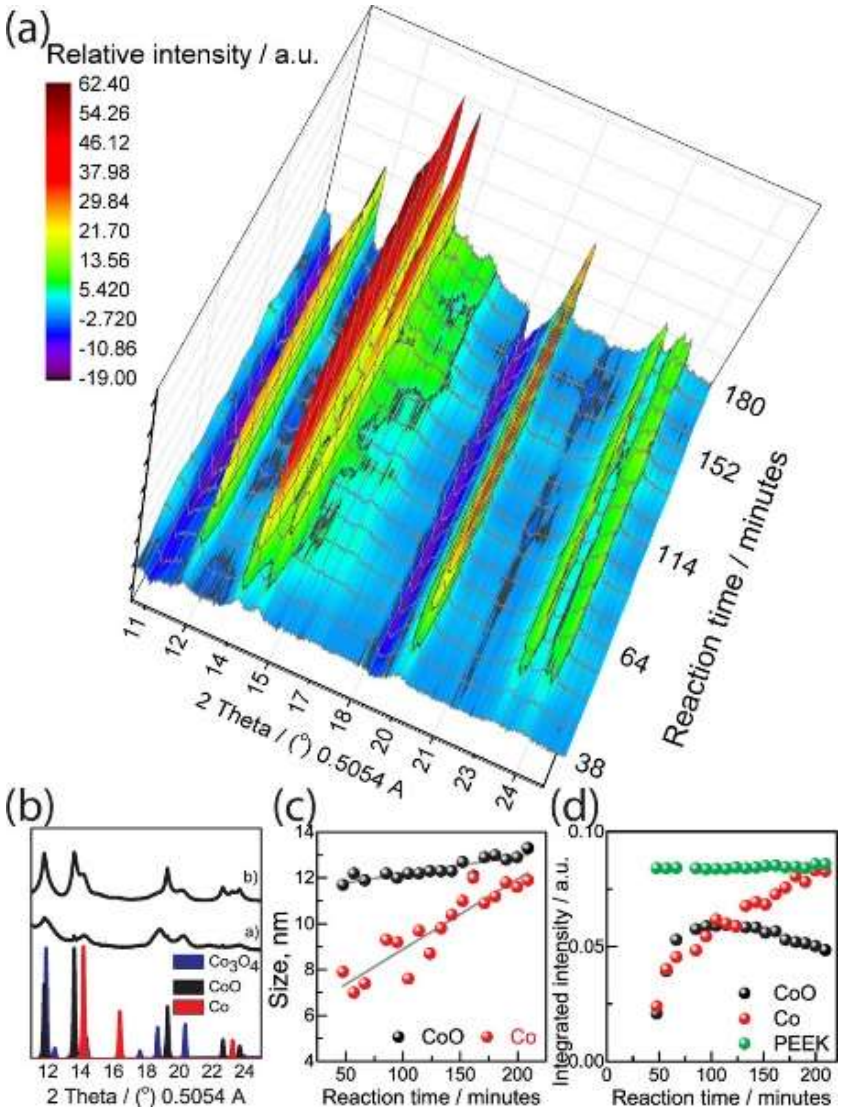

*Relative changes of the diffraction patterns during the reaction at 140 °C, showing phase transformations. Reprinted with permission from M. Staniuk, O. Hirsch, N. Kränzlin, R. Böhlen, W. van Beek, P.M. Abdala, D. Koziej, Puzzling, Chemistry of Materials **26** (2014) 2086–2094. Copyright 2014 American Chemical Society [21].*

Grote *et al.* used this same reactor cell in order to provide a comprehensive study on the **evolution of CoO nano-assemblies in solution** [22]. They used a wide range of X-ray measurements - **XAS**, **PDF**, **SAXS**, and laboratory XRD - in order to characterize the nanoparticles' mean size, their superstructure, and the molecular assemblies of the Co acetylacetonate. This multiscale characterisation enabled a better understanding of the complex evolution of those nanoparticles (figure below), and thereby improved control of the synthetization process.

Experiments were performed at the Swedish Materials Science beamline, **P21.1** branch (for total scattering - PDF), at the **P03** beamline at **Petra III** (for SAXS) and at the **ID26** and **BM14** beamline at **ESRF** (for XAS).

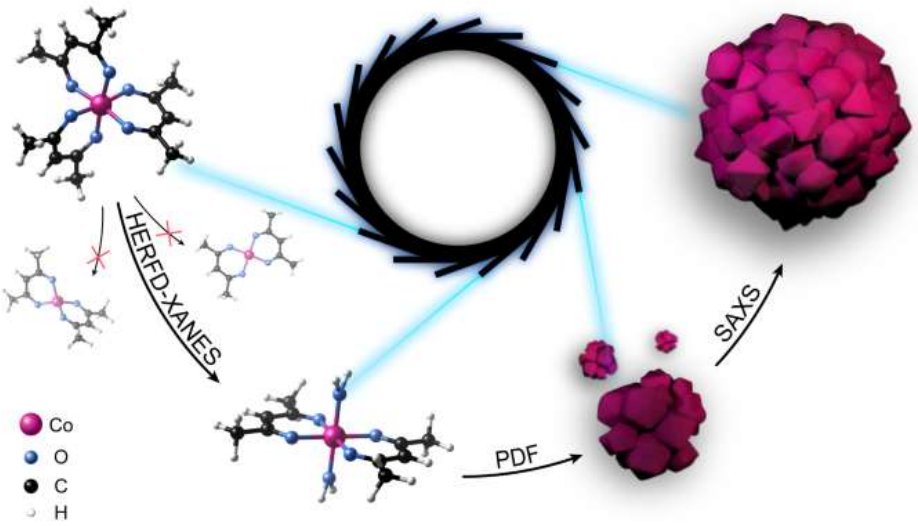

"Complementary X-ray spectroscopic and scattering methods enable the bridging of the studies of the reaction mechanism from molecular- to macro- length scales" from Grote et al. 2021 [22], CC BY (Open access article).

Further information about the sample environment:

Description article: [21] M. Staniuk *et al.* (2014) *Chem. Mater.*, Vol.26, No.6, p.2086-2094. (https://doi.org/10.1021/cm500090r)

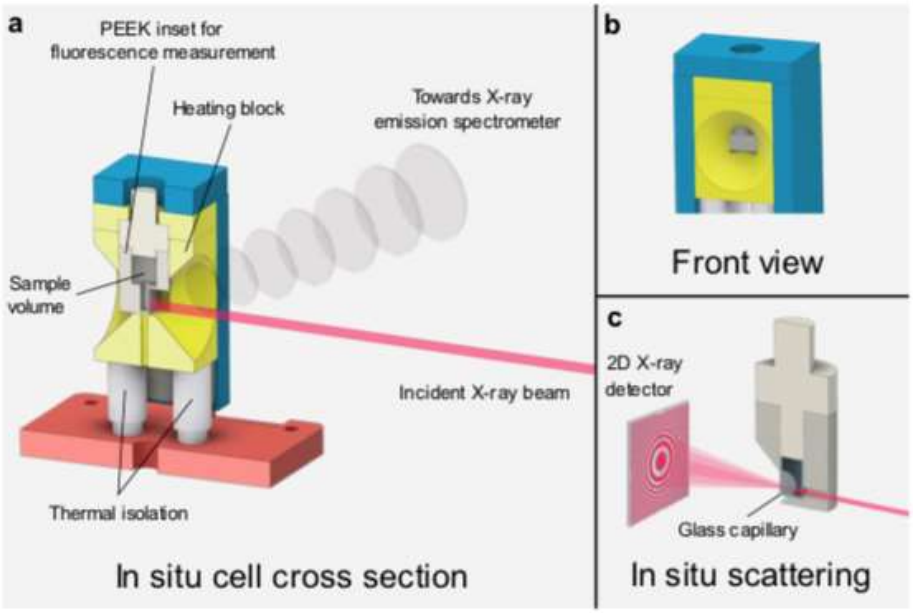

Schematic of the sample environment and experimental setup, from Grote et al. 2021 [22] (in additional materials), CC BY (Open access article).

3.3. Catalysis

UFO chamber mini reactor | DESY Nanolab

In their study, Shipilin *et al.* studied the **carbide formation on an iron-based catalyst**. They used *in-situ* X-Ray Photoelectron Spectroscopy (XPS) and *in-situ* **SXRD** with increasing **temperature up to 350 °C at various pressure levels** (85, 550 and 700 mbar). The UFO mini reactor chamber was used for SXRD only. The UFO chamber was **vacuumed first,** and then pressure was controlled by an **inlet gas flow** available on the UFO chamber. The study enabled an understanding of which crystalline iron carbides were forming at different temperatures as well as their dependences on the pressure and gas feed composition.

The experiments where performed at the Swedish Materials Science beamlines, **P21.2** branch, (for SXRD) and the **P22** (for XPS) beamline at PETRA III [23].

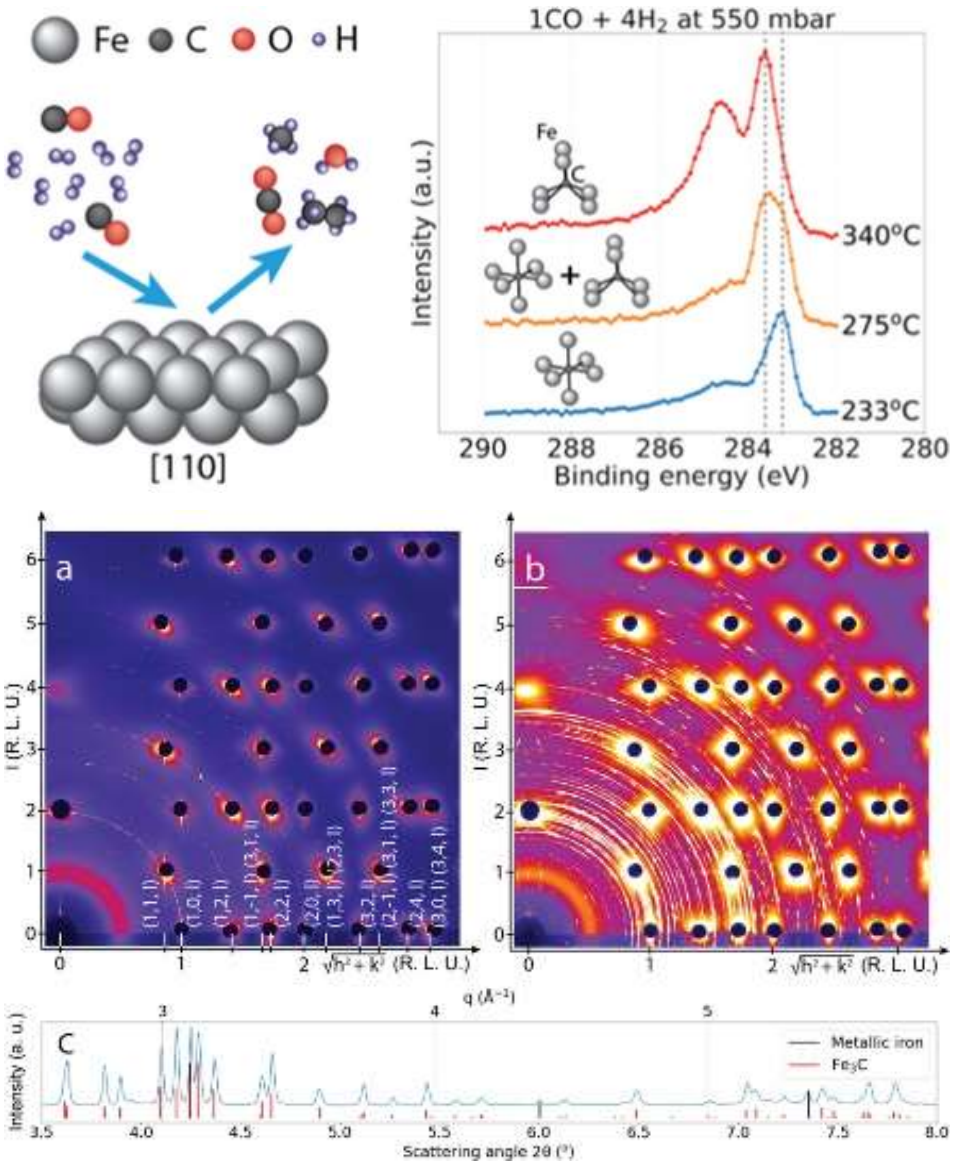

In-situ XPS (left) and SXRD (right) performed at different temperature, pressure and gas feed mixture, showing the evolution of the Fe-carbides at different temperatures, from Shipilin et al. 2022 [23], CC BY (Open access article).

Further information about the sample environment:
DESY Nanolab website: Nanolab sample environment description.

3.4. Thin film deposition

Magnetron sputtering and cathodic arc ultra-high vacuum deposition system | Linköping University (Sweden)

In their publication describing the sample environment, Schroeder *et al.* performed a demonstration measurement studying the **growth of a $Zr_{0.75}Al_{0.25}N$ coating** on a Si substrate **[24]**. The Si substrate was heated up to 700 °C and the deposition chamber pressure was set to **5 mTorr** with an **atmosphere of 10%N_2/90%Ar,** the background pressure before the introduction of the atmosphere gas was 2.0×10^{-9} Torr. A **deposition rate of 20 nm/min** was applied, using a $Zr_{0.75}Al_{0.25}$ target. Each **SXRD** image was acquired during a full 360° rotation of the sample. This measurements enabled observation of the thin film growth together with the characterisation of its crystalline structure.

Eriksson *et al.* used the same deposition system for the deposition of **B_4C-doped Ni/Ti multilayer neutron mirrors [25]**. The films were deposited on constantly rotating Si substrates. Depositions were performed without heating (even if available), at the ambient growth temperature. A **3 mTorr** atmosphere of high purity **Ar** was set and **3 sputter sources** were used in confocal geometry to realize the deposition. **XRD *in-situ*** measurement was performed, which enabled tracking of the crystallization of Ni and Ti over the deposition process, with and without B_4C addition, revealing the efficiency of B_4C to hinder crystallization of Ni and Ti. This amorphization of the Ni/Ti multilayers is beneficial for the performance of the produced neutron mirrors.

Both sets of experiments were performed at the **P07** beamline at PETRA III.

Further information about the sample environment:
Description article: [24] J.L. Schroeder *et al.* (2015) *Review of Scientific Instruments*, Vol.86, No. 095113. (https://doi.org/10.1063/1.4930243)

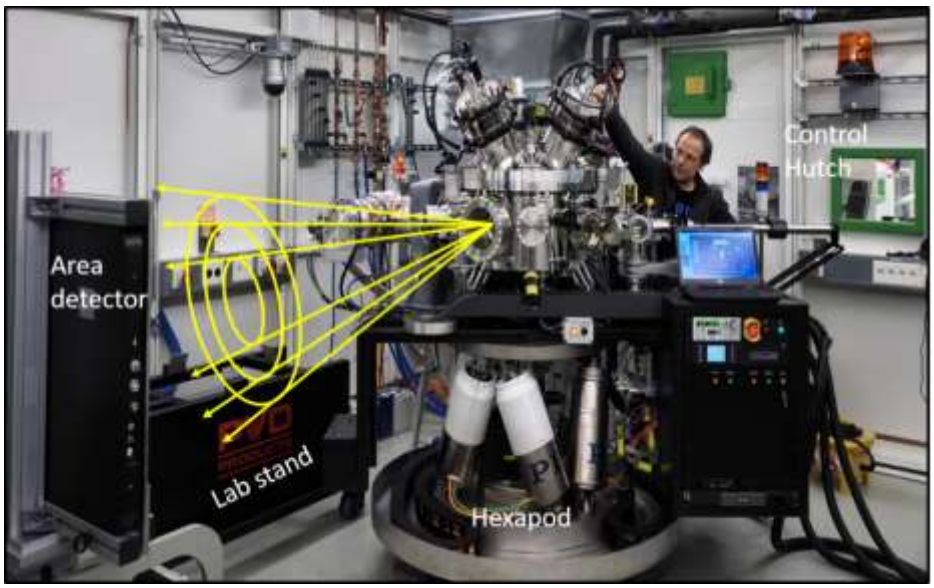

The deposition system and experimental setup, courtesy of Prof. Jens Birch.

3.5.Mechanical response of materials

Cutting tool X-cut | Linköping University (Sweden)

The article from Rogström *et al.* describes this sample environment and provides a demonstration of its research capabilities. This work aimed at measuring the stress and temperature at the cutting edge of a **TiAlNbN coated WC-Co cutting tool** during cutting of carbon steel **[26]**. The workpiece rotation speed was set to **800 rpm** and the feed rate of the cutting was set to the maximum of **0.3 mm/revolution**. **In *operando* XRD** where performed during cutting and enabled determination of in-plane stresses and temperatures through the variation of the lattice parameters of the phases present in the cutting tool.

Experiments were performed at the **P07** beamline at PETRA III.

Further information about the sample environment:

Description article: [26] L. Rogström *et al.* (2019) *Review of Scientific Instruments*, Vol.90, No. 103901 (https://doi.org/10.1063/1.5091766).

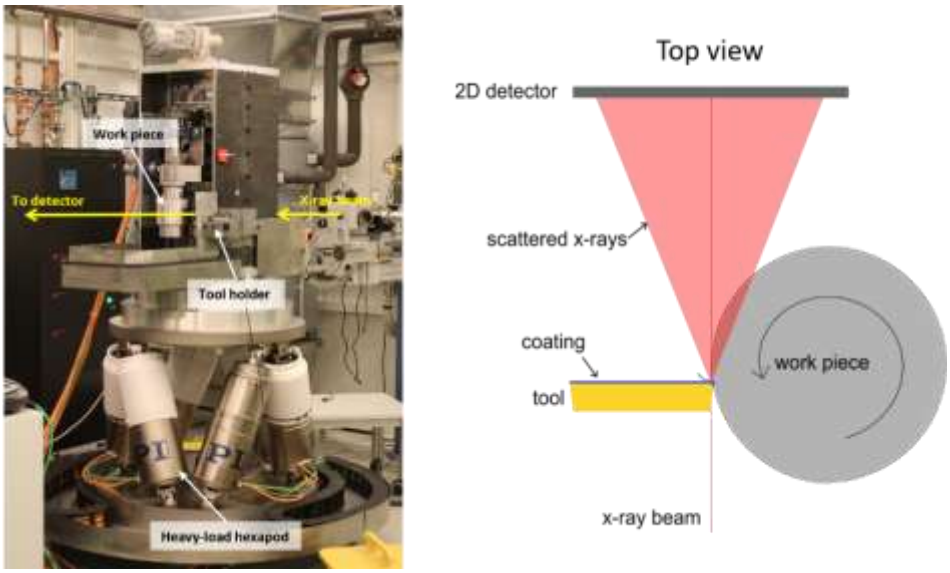

Schematic and picture of the sample environment, courtesy of Prof. Jens Birch.

Compact uniaxial load frame | P21.2

The **P21.2 branch** of the Swedish beamline have load frame available to conduct in-situ uniaxial **loading up to 5 kN load**, with **displacement control only**, currently **without heating capacity**. Depending on the material investigated, this device could enable measurement of lattice strain evolution of different crystalline phases during loading, similar to Miao et al. who looked at the lattice strain of matrix phases (austenite and martensite) and precipitates (TiN and Y-Al-O nano-oxides) in oxide dispersion strengthened austenitic steel **[27]**. These experiments were conducted at the APS synchrotron on the 1-ID beamline. Another possibility would be to quantify deformation-induced phase transformation, as performed by Choi et al. with an austenitic steel, displaying transformation-induced plasticity, who observed the evolution of the austenite phase fraction as function of the applied strain **[28]**. These measurements were performed at the APS synchrotron using the 11-ID-C beamline.

Other possibilities of measurements may be available for this instrument, and the interested reader is encouraged to discuss with the beamline scientists of P21.2 to seek further information and advice.

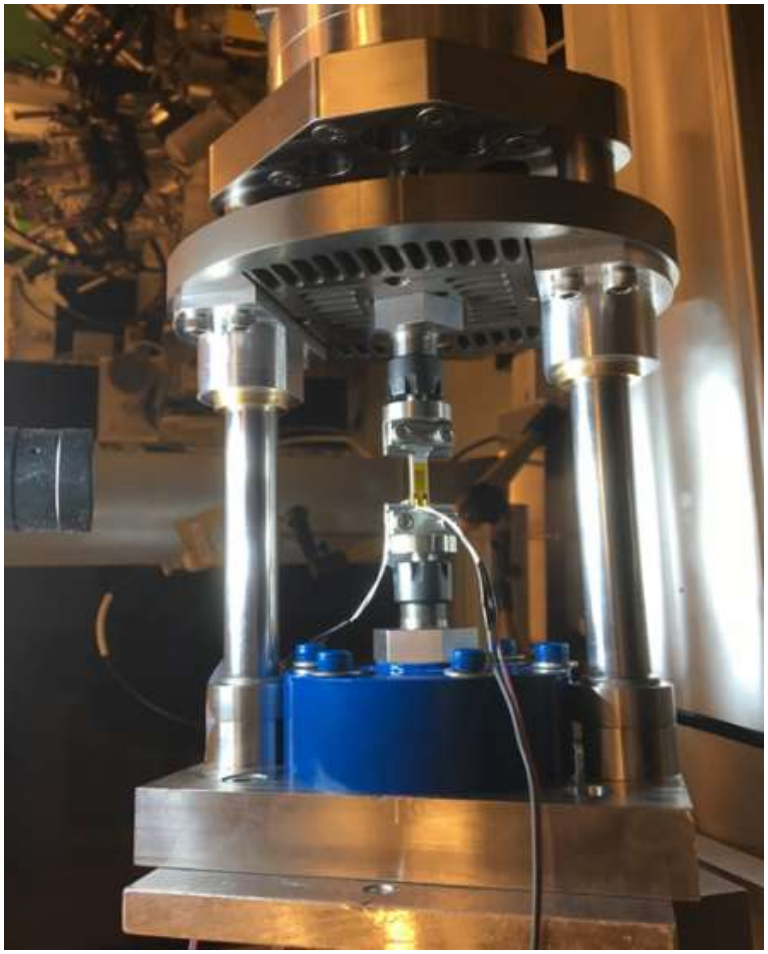

Picture of the load frame at P21.2, courtesy of Dr. Ulrich Lienert.

3.6. Levitation

Mobile ElectroMagnetic Levitation (EML) facility | IFW Dresden (Germany)

In their work, Andreoli *et al.* studied the solidification of **CoCrFeNi HEA as well as CrFeNi** and **CoCrNi ternary alloys [29], also NbTiVZr HEA** has been studied **[30]**. The EML facility was used to levitate the samples and heat them by induction heating using a water-cooled copper coil with an inner diameter of 1 mm, up to a **temperature higher than 2000 K** (higher than the melting temperature). The samples were placed in the P21.1 scattering chamber, under a high purity He atmosphere at pressure of 500-700 mbar. The scattering chamber of P21.1 allows work under vacuum or in a He atmosphere, it has an angular opening of 30° and various sample environments such as heating devices can be placed inside (see P21.1 website in section 4 for more information) The cooling was performed utilizing a He jet with a flux of 25 l/min. ***In-situ* XRD** measurements were performed in order to follow the crystallization of the samples with respect to the temperature during solidification and depending on the alloy composition.

Experiments were performed at the Swedish Materials Science beamline, **P21.1** branch.

Further information about the sample environment:

Technical report: [31] O. Shuleshova (2017) IFW Dresden Annual report 2017. (https://www.ifw-dresden.de/uploads/users/10/uploads/files/JB_2017.pdf)

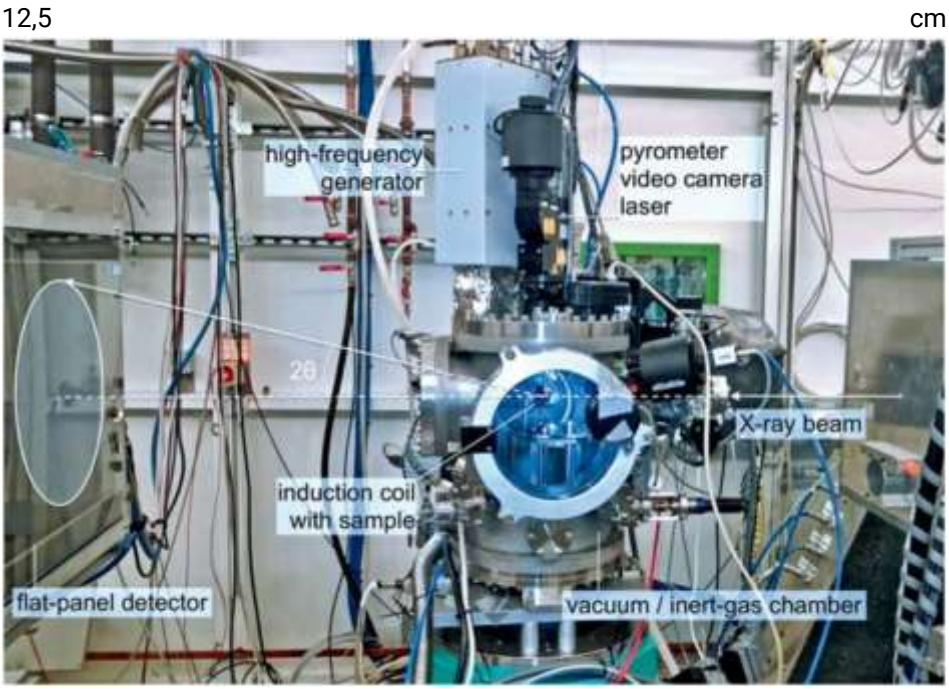

Mobile ElectroMagnetic Levitation facility inside the P21.1 scattering chamber (called "vacuum / inert-gas chamber" in the picture), courtesy of Leibniz Institute for Solid State and Materials Research Dresden [31].

Aerodynamic Levitation (ADL) system | Institut für Materialphysik im Weltraum (Germany)

Schraut *et al.* studied the **solidification of the CaO–SiO_2 system**, with different CaO amounts (between 70 and 80 mol%). They used the ADL device in order to melt the samples and observed their solidification upon cooling at **cooling rates** ranging between **300 K/s** and **1 K/s** by ***in-situ* XRD** measurements **[32]**. The sample was **levitated by the ADL system using a gas jet** coming from a converging-diverging nozzle and **heated by 2 CO_2 lasers** up to melting. The atmosphere was pure Ar gas or a mixture of Ar and O2 gas to generate reducing or oxidizing atmosphere respectively. The ***in-situ* XRD** measurements enabled observations of which crystalline phases formed as well as the dependence of the phase formation on the reducing or oxidizing atmosphere employed, different cooling rates, and the different mixture of CaO–SiO_2 investigated.

Experiments were conducted at the Swedish Materials Science beamline, **P21.1** branch.

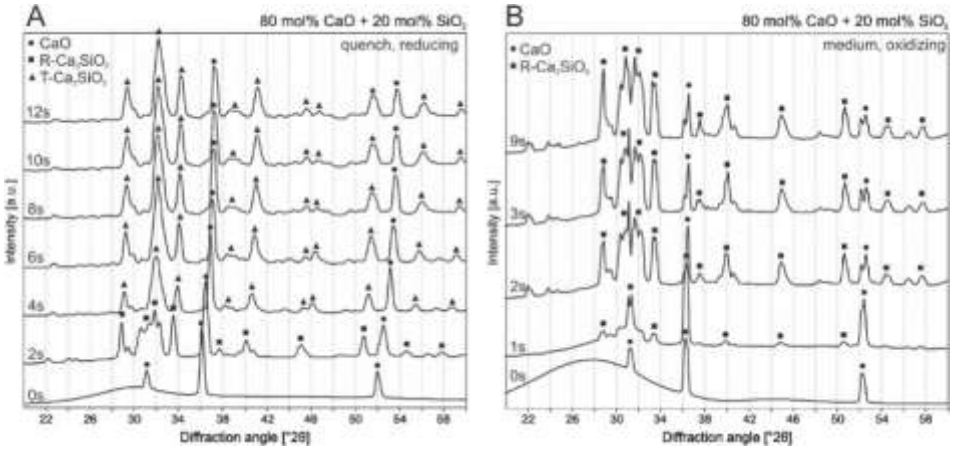

XRD diffraction patterns at different stages of the cooling, using a reducing (A) and oxidizing (B) atmosphere, from Schraut et al. [32], CC BY (Open access article).

Further information about the sample environment:

Description article: [33] F. Kargl *et al.* (2015) Int. J. Microgravity Sci. Appl. Vol.32 No.2, p.320212. (https://doi.org/10.15011/ijmsa.32.320212)

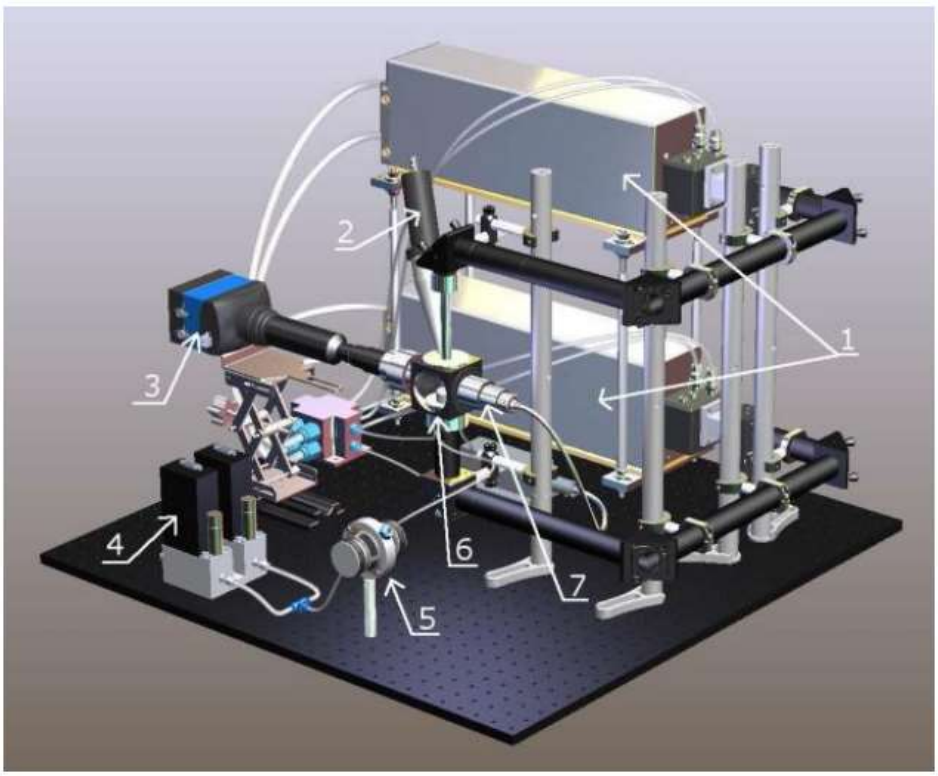

"Schematic drawing of the levitation setup. 1) CO_2 lasers, 2) pyrometer, 3) high-speed camera, 4) mass-flow controller, 5) acoustic excitation system, 6) levitation chamber, and 7) diode laser for backlighting" from F. Kargl et al. 2015 [33], CC BY (Open access article).

4. Useful links

P21.1 Sample environments

https://photon-science.desy.de/facilities/petra_iii/beamlines/p21_swedish_materials_science/p211_high_energy_x_ray_diffraction_for_physics_and_chemistry/sample_environments/index_eng.html

P21.2 Website

https://photon-science.desy.de/facilities/petra_iii/beamlines/p21_swedish_materials_science/p212_diffraction__imaging/index_eng.html

Sample Environment and Extreme Conditions Science Infrastructure (ECSI) (Pool equipment sample environments of Petra III)

https://photon-science.desy.de/facilities/on_site_infrastructure/laboratories_technical_infrastructure_shift_service/sample_environment_and_ecsi/index_eng.html

DESY Nanolab Sample environments

https://photon-science.desy.de/research/research_teams/x_ray_physics_and_nanoscience/desy_nanolab_instrumentation/x_ray_diffraction/index_eng.html

Note. These links were accessed in January 2023.

5. Useful contacts

P21.1 team

https://photon-science.desy.de/facilities/petra_iii/beamlines/p21_swedish_materials_science/p211_high_energy_x_ray_diffraction_for_physics_and_chemistry/contact__staff/index_eng.html

Scientist in charge: martin.v.zimmermann@desy.de

P21.2 team

https://photon-science.desy.de/facilities/petra_iii/beamlines/p21_swedish_materials_science/p212_diffraction__imaging/contact__staff/index_eng.html

Scientist in charge: ulrich.lienert@desy.de

Sample Environment and Extreme Conditions Science Infrastructure (ECSI) of Petra III

https://photon-science.desy.de/facilities/on_site_infrastructure/laboratories_technical_infrastructure_shift_service/sample_environment_and_ecsi/people/index_eng.html

Main contact person: anita.ehnes@desy.de

DESY Nanolab

https://photon-science.desy.de/facilities/desy_nanolab/index_eng.html

DESY Nanolab email: nanolab@desy.de

Main contact person: andreas.stierle@desy.de

Note. These links were accessed in January 2023.

6. Acknowledgements

This work was conducted under the auspices of the Center for X-rays in Swedish Materials Science (CeXS). CeXS acts as the academic host of the PETRA III Swedish Materials Science beamline. CeXS is co-funded by VR and the partners KTH Royal Institute of Technology and Linköping University as well as the affiliate partner Uppsala University. The authors gratefully acknowledge the support of these organisations.

The authors acknowledge the research groups who have developed their own sample environments, the beamline scientists at the PETRA III Swedish Materials Science beamline and ECSI (PETRA III pool equipment) and DESY Nanolab for discussions and providing information during the preparation of this report.

7. References

[1] H.-R. Jiang, J.-Y. Hu, N. Neuber, B. Bochtler, B. Adam, S.S. Riegler, M. Frey, L. Ruschel, W.-F. Lu, A.-H. Feng, R. Busch, J. Shen, Effect of sulfur on the glass-forming ability, phase transformation, and thermal stability of Cu-Zr-Al bulk metallic glass, Acta Materialia. 212 (2021) 116923. https://doi.org/10.1016/j.actamat.2021.116923.

[2] L. Weissitsch, S. Wurster, A. Paulischin, M. Stückler, R. Pippan, A. Bachmaier, Nanocrystalline FeCr alloys synthesised by severe plastic deformation – A potential material for exchange bias and enhanced magnetostriction, Journal of Magnetism and Magnetic Materials. 534 (2021) 168017. https://doi.org/10.1016/j.jmmm.2021.168017.

[3] S. Wurster, M. Stückler, L. Weissitsch, T. Müller, A. Bachmaier, Microstructural Changes Influencing the Magnetoresistive Behavior of Bulk Nanocrystalline Materials, Applied Sciences. 10 (2020) 5094. https://doi.org/10.3390/app10155094.

[4] N.L.N. Broge, M. Bondesgaard, F. Søndergaard-Pedersen, M. Roelsgaard, B.B. Iversen, Autocatalytic Formation of High-Entropy Alloy Nanoparticles, Angewandte Chemie International Edition. 59 (2020) 21920–21924. https://doi.org/10.1002/anie.202009002.

[5] J. Becker, M. Bremholm, C. Tyrsted, B. Pauw, K.M.Ø. Jensen, J. Eltzholt, M. Christensen, B.B. Iversen, Experimental setup for in situ X-ray SAXS/WAXS/PDF studies of the formation and growth of nanoparticles in near- and supercritical fluids, J Appl Cryst. 43 (2010) 729–736. https://doi.org/10.1107/S0021889810014688.

[6] I.-E. Benrabah, H.. V. Landeghem, F. Bonnet, B. Denand, G. Geandier, A. Deschamps, Solute drag modeling for ferrite growth kinetics during precipitation experiments, Acta Materialia. (2021) 117364. https://doi.org/10.1016/j.actamat.2021.117364.

[7] I.-E. Benrabah, F. Bonnet, B. Denand, A. Deschamps, G. Geandier, H.P. Van Landeghem, High-throughput compositional mapping of phase transformation kinetics in low-alloy steel, Applied Materials Today. 23 (2021) 100997. https://doi.org/10.1016/j.apmt.2021.100997.

[8] B. Denand, M. Dehmas, E. Aeby-Gautier, B. Christophe, G. Géandier, S. Jean-Pierre, PORTABLE ANALYSIS KILN FOR RADIATION LINE, 2019. https://hal.univ-lorraine.fr/hal-03451741 (accessed November 10, 2022).

[9] J. Orava, S. Balachandran, X. Han, O. Shuleshova, E. Nurouzi, I. Soldatov, S. Oswald, O. Gutowski, O. Ivashko, A.-C. Dippel, M. v. Zimmermann, Y.P. Ivanov, A.L. Greer, D. Raabe, M. Herbig, I. Kaban, In situ correlation between metastable phase-transformation mechanism and kinetics in a metallic glass, Nat Commun. 12 (2021) 2839. https://doi.org/10.1038/s41467-021-23028-9.

[10] R. Hermann, W. Löser, H.G. Lindenkreuz, W. Yang-Bitterlich, C. Mickel, A. Diefenbach, S. Schneider, W. Dreier, Metastable phase formation in undercooled Fe-Co melts under terrestrial and parabolic flight conditions, Microgravity Sci. Technol. 19 (2007) 5–10. https://doi.org/10.1007/BF02870982.

[11] J. Orava, K. Kosiba, X. Han, I. Soldatov, O. Gutowski, O. Ivashko, A.-C. Dippel, M. v. Zimmermann, A. Rothkirch, J. Bednarcik, U. Kühn, H. Siegel, S. Ziller, A. Horst, K. Peukert, R. Voigtländer, D. Lindackers, I. Kaban, Fast-current-heating devices to study in situ phase formation in metallic glasses by using high-energy synchrotron radiation, Review of Scientific Instruments. 91 (2020) 073901. https://doi.org/10.1063/5.0005732.

[12] F. Zhang, J. Evertsson, F. Bertram, L. Rullik, F. Carla, M. Långberg, E. Lundgren, J. Pan, Integration of electrochemical and synchrotron-based X-ray techniques for in-situ investigation of aluminum anodization, Electrochimica Acta. 241 (2017) 299–308. https://doi.org/10.1016/j.electacta.2017.04.154.

[13] T. Weber, V. Vonk, D. Escalera-López, G. Abbondanza, A. Larsson, V. Koller, M.J.S. Abb, Z. Hegedüs, T. Bäcker, U. Lienert, G.S. Harlow, A. Stierle, S. Cherevko, E. Lundgren, H. Over, Operando Stability Studies of Ultrathin Single-Crystalline IrO2(110) Films under Acidic Oxygen Evolution Reaction Conditions, ACS Catal. 11 (2021) 12651–12660. https://doi.org/10.1021/acscatal.1c03599.

[14] M.L. Foresti, A. Pozzi, M. Innocenti, G. Pezzatini, F. Loglio, E. Salvietti, A. Giusti, F. D'Anca, R. Felici, F. Borgatti, In situ X-ray analysis under controlled potential conditions: An innovative setup and its application to the investigation of ultrathin films electrodeposited on Ag(111), Electrochimica Acta. 51 (2006) 5532–5539. https://doi.org/10.1016/j.electacta.2006.02.031.

[15] C. Örnek, T. Müller, B.M. Şeşen, U. Kivisäkk, F. Zhang, M. Långberg, U. Lienert, A. Jeromin, T.F. Keller, E. Lundgren, J. Pan, Hydrogen-Induced Micro-Strain Evolution in Super Duplex Stainless Steel—Correlative High-Energy X-Ray Diffraction, Electron Backscattered Diffraction, and Digital Image Correlation, Front. Mater. 8 (2022) 793120. https://doi.org/10.3389/fmats.2021.793120.

[16] C. Örnek, T. Müller, U. Kivisäkk, F. Zhang, M. Långberg, U. Lienert, K.-H. Hwang, E. Lundgren, J. Pan, Operando time- and space-resolved high-energy X-ray diffraction measurement to understand hydrogen-microstructure interactions in duplex stainless steel, Corrosion Science. 175 (2020) 108899. https://doi.org/10.1016/j.corsci.2020.108899.

[17] W. Linpé, L. Rämisch, G. Abbondanza, A. Larsson, S. Pfaff, L. Jacobse, J. Zetterberg, L. Merte, A. Stierle, Z. Hegedues, U. Lienert, E. Lundgren, G.S. Harlow, Revisiting Optical Reflectance from Au(111) Electrode Surfaces with Combined High-Energy Surface X-ray Diffraction, J. Electrochem. Soc. 168 (2021) 096511. https://doi.org/10.1149/1945-7111/ac2702.

[18] W. Linpé, G.S. Harlow, A. Larsson, G. Abbondanza, L. Rämisch, S. Pfaff, J. Zetterberg, J. Evertsson, E. Lundgren, An electrochemical cell for 2-dimensional surface optical reflectance during anodization and cyclic voltammetry, Review of Scientific Instruments. 91 (2020) 044101. https://doi.org/10.1063/1.5133905.

[19] S. Pfaff, A. Larsson, D. Orlov, G.S. Harlow, G. Abbondanza, W. Linpé, L. Rämisch, S.M. Gericke, J. Zetterberg, E. Lundgren, Operando Reflectance Microscopy on Polycrystalline Surfaces in Thermal Catalysis, Electrocatalysis, and Corrosion, ACS Appl. Mater. Interfaces. 13 (2021) 19530–19540. https://doi.org/10.1021/acsami.1c04961.

[20] S. Galeski, T. Ehmcke, R. Wawrzyńczak, P.M. Lozano, K. Cho, A. Sharma, S. Das, F. Küster, P. Sessi, M. Brando, R. Küchler, A. Markou, M. König, P. Swekis, C. Felser, Y. Sassa, Q. Li, G. Gu, M.V. Zimmermann, O. Ivashko, D.I. Gorbunov, S. Zherlitsyn, T. Förster, S.S.P. Parkin, J. Wosnitza, T. Meng, J. Gooth, Origin of the quasi-quantized Hall effect in ZrTe5, Nat Commun. 12 (2021) 3197. https://doi.org/10.1038/s41467-021-23435-y.

[21] M. Staniuk, O. Hirsch, N. Kränzlin, R. Böhlen, W. van Beek, P.M. Abdala, D. Koziej, Puzzling Mechanism behind a Simple Synthesis of Cobalt and Cobalt Oxide Nanoparticles: In Situ Synchrotron X-ray Absorption and Diffraction Studies, Chem. Mater. 26 (2014) 2086–2094. https://doi.org/10.1021/cm500090r.

[22] L. Grote, C.A. Zito, K. Frank, A.-C. Dippel, P. Reisbeck, K. Pitala, K.O. Kvashnina, S. Bauters, B. Detlefs, O. Ivashko, P. Pandit, M. Rebber, S.Y. Harouna-Mayer, B. Nickel, D. Koziej, X-ray studies bridge the molecular and macro length scales during the emergence of CoO assemblies, Nat Commun. 12 (2021) 4429. https://doi.org/10.1038/s41467-021-24557-z.

[23] M. Shipilin, D. Degerman, P. Lömker, C.M. Goodwin, G.L.S. Rodrigues, M. Wagstaffe, J. Gladh, H.-Y. Wang, A. Stierle, C. Schlueter, L.G.M. Pettersson, A. Nilsson, P. Amann, In Situ Surface-Sensitive Investigation of Multiple Carbon Phases on Fe(110) in the Fischer–Tropsch Synthesis, ACS Catal. 12 (2022) 7609–7621. https://doi.org/10.1021/acscatal.2c00905.

[24] J.L. Schroeder, W. Thomson, B. Howard, N. Schell, L.-Å. Näslund, L. Rogström, M.P. Johansson-Jõesaar, N. Ghafoor, M. Odén, E. Nothnagel, A. Shepard, J. Greer, J. Birch, Industry-relevant magnetron sputtering and cathodic arc ultra-high vacuum deposition system for in situ x-ray diffraction studies of thin film growth using high energy synchrotron radiation, Review of Scientific Instruments. 86 (2015) 095113. https://doi.org/10.1063/1.4930243.

[25] F. Eriksson, N. Ghafoor, D. Ostach, N. Schell, J. Birch, Ion-assisted magnetron sputter deposition of B4C-doped Ni/Ti multilayer mirrors, in: Advances in X-Ray/EUV Optics and Components XIII, SPIE, 2018: pp. 40–43. https://doi.org/10.1117/12.2317742.

[26] L. Rogström, Y.H. Chen, M.P. Johansson Jõesaar, J. Eriksson, M. Fallqvist, J.M. Andersson, N. Schell, M. Odén, J. Birch, A custom built lathe designed for in operando high-energy x-ray studies at industrially relevant cutting parameters, Review of Scientific Instruments. 90 (2019) 103901. https://doi.org/10.1063/1.5091766.

[27] Y. Miao, K. Mo, Z. Zhou, X. Liu, K.-C. Lan, G. Zhang, M.K. Miller, K.A. Powers, J. Almer, J.F. Stubbins, In situ synchrotron tensile investigations on the phase responses within an oxide dispersion-strengthened (ODS) 304 steel, Materials Science and Engineering: A. 625 (2015) 146–152. https://doi.org/10.1016/j.msea.2014.12.017.

[28] K.S. Choi, W.N. Liu, X. Sun, M.A. Khaleel, Y. Ren, Y.D. Wang, Advanced Micromechanical Model for Transformation-Induced Plasticity Steels with Application of In-Situ High-Energy X-Ray Diffraction Method, Metall Mater Trans A. 39 (2008) 3089–3096. https://doi.org/10.1007/s11661-008-9649-4.

[29] A.F. Andreoli, O. Shuleshova, V.T. Witusiewicz, Y. Wu, Y. Yang, O. Ivashko, A.-C. Dippel, M. v. Zimmermann, K. Nielsch, I. Kaban, In situ study of non-equilibrium solidification of CoCrFeNi high-entropy alloy and CrFeNi and CoCrNi ternary suballoys, Acta Materialia. 212 (2021) 116880. https://doi.org/10.1016/j.actamat.2021.116880.

[30] A.F. Andreoli, R.G. Mendes, V.T. Witusiewicz, O. Shuleshova, M.A. van Huis, K. Nielsch, I. Kaban, Phase constitution and microstructure of the NbTiVZr refractory high-entropy alloy solidified upon different processing, Acta Materialia. 221 (2021) 117416. https://doi.org/10.1016/j.actamat.2021.117416.

[31] O. Shuleshova, IFW Dresden Annual Report 2017, 2017. https://www.ifw-dresden.de/uploads/users/10/uploads/files/JB_2017.pdf.

[32] K. Schraut, F. Kargl, C. Adam, O. Ivashko, In situ synchrotron XRD measurements during solidification of a melt in the CaO–SiO2 system using an aerodynamic levitation system, J. Phys.: Condens. Matter. 33 (2021) 264003. https://doi.org/10.1088/1361-648X/abf7e1.

[33] F. Kargl, C. Yuan, G.N. Greaves, Aerodynamic Levitation: Thermophysical Property Measurements of Liquid Oxides, International Journal of Microgravity Science and Application. 32 (2015) 320212. https://doi.org/10.15011/ijmsa.32.320212.

KTH

UPPSALA UNIVERSITET

LINNÉUNIVERSITETET

Swedish Research Council

cexs.kth.se